



LUND UNIVERSITY  
Faculty of Medicine

---

# LUP

*Lund University Publications*

Institutional Repository of Lund University

---

This is an author produced version of a paper published in Bone. This paper has been peer-reviewed but does not include the final publisher proof-corrections or journal pagination.

Citation for the published paper:  
Sofia Lagerholm, Hee-Bok Park, Holger Luthman,  
Mats A Nilsson, Fiona McGuigan, Maria Swanberg,  
Kristina Åkesson

"Genetic loci for bone architecture determined by three-dimensional CT in crosses with the diabetic GK rat."

Bone 2010 Aug 10

<http://dx.doi.org/10.1016/j.bone.2010.08.003>

Access to the published version may require journal subscription.

Published with permission from: Elsevier

# Genetic loci for bone architecture determined by three-dimensional CT in crosses with the diabetic GK rat

Sofia Lagerholm<sup>1</sup>, Hee-Bok Park<sup>2</sup>, Holger Luthman<sup>2</sup>, Mats Nilsson<sup>3</sup>, Fiona McGuigan<sup>1</sup>, Maria Swanberg<sup>1</sup>, Kristina Åkesson<sup>1,4</sup>

1, Lund University, Department of Clinical Sciences-Malmö, Clinical and Molecular Osteoporosis Unit<sup>1</sup>, Medical Genetics Unit<sup>2</sup> Medical Radiation Physics<sup>3</sup> and Department of Orthopedics<sup>4</sup>, Malmö, Sweden

Corresponding author:

Holger Luthman

Lund University

Entrance 72, Bldn. 91, Fl. 11, UMAS

SE-205 02 Malmö, Sweden

Tel: +46 40 39 11 58

Fax: +46 40 39 12 22

Holger.Luthman@med.lu.se

Sofia.Lagerholm@med.lu.se

Hee-Bok.Park@med.lu.se

Holger.Luthman@med.lu.se

Mats.Nilsson@med.lu.se

Fiona.McGuigan@med.lu.se

Maria.Swanberg@med.lu.se

Kristina.Akesson@med.lu.se

**Key words:** QTL; CT; Bone size; GK rat; Reciprocal cross

## **Abstract**

The F344 rat carries alleles contributing to bone fragility while the GK rat spontaneously develops type-2 diabetes. These characteristics make F344 x GK crosses well suited for the identification of genes related to bone size and allow for future investigation on the association with type-2 diabetes. The aim of this study was to identify quantitative trait loci (QTLs) for bone size phenotypes measured by a new application of three-dimensional computed tomography (3DCT) and to investigate the effects of sex- and reciprocal cross.

Tibia from male and female GK and F344 rats, representing the parental, F1 and F2 generations, were examined with 3DCT and analyzed for: total and cortical volumetric BMD, straight and curved length, peri- and endosteal area at mid-shaft. F2 progeny (108 male and 98 female) were genotyped with 192 genome-wide microsatellite markers (average distance 10 cM). Sex- and reciprocal cross-separated QTL analyses were performed for the identification of QTLs linked to 3DCT phenotypes and true interactions were confirmed by likelihood ratio analysis in all F2 animals.

Several genome-wide significant QTLs were found in the sex- and reciprocal cross-separated progeny on chromosomes (chr) 1, 3, 4, 9, 10, 14, and 17. Overlapping QTLs for both males and females in the (GK×F344)F2 progeny were located on chr 1 (39-67 cM). This region confirms previously reported pQCT QTLs and overlaps loci for fasting glucose. Sex separated linkage analysis confirmed a male specific QTL on chr 9 (67-82 cM) for endosteal area at the fibula site. Analyses separating the F2 population both by sex and reciprocal cross identified cross specific QTLs on chr 14 (males) and chr 3 and 4 (females). Two loci, chr 4 and 6, are unique to 3DCT and separate from pQCT generated loci.

The 3DCT method was highly reproducible and provided high precision measurements of bone size in the rat enabling identification of new sex- and cross-specific loci. The QTLs on chr 1 indicate potential genetic association between bone-related phenotypes and traits affecting type-2 diabetes. The results illustrate the complexity of the genetic architecture of bone size phenotypes, and demonstrate the importance of complementary methods for bone analysis.

## ***Introduction***

Osteoporosis is characterised by compromised bone strength leading to increased risk of fracture and is a multifactorial disease influenced by genes and environmental factors [1]. After extensive efforts, genome-wide association studies are finally yielding in identifying candidate markers for phenotypes associated with osteoporosis (BMD) [2]. Several determinants apart from bone density, such as bone size, skeletal macrostructure, cortical geometry and trabecular microarchitecture affect bone strength and the ability to resist fracture [3]. Analysis of these inter-related phenotypes enhances the likelihood of identifying genes with pleiotropic effects on bone [4]. The use of animal models as a complement to studies in human populations permit identification of candidate genes for additional phenotypes related to bone structure and strength. Inbred rodent strains have been established as valuable models for dissecting the genetic regulation of bone, and several chromosomal regions linked to bone geometry, biomechanics and bone density in distinct trabecular or cortical bone compartments have been identified [3, 5-7].

Differences in bone structure, BMD and fragility phenotypes between inbred strains of rats have been identified including the non-diabetic F344 and the type-2 diabetic GK strain [8-10]. In experimental crosses, F344 has been shown to carry alleles that cause overall skeletal fragility [6, 11-13]. The GK strain displays hyperglycemia and impaired insulin secretion and is a well characterised genetic model for type-2 diabetes [14, 15]. Abnormalities in the insulin-like growth factor (IGF)-system were also recently reported to affect bone in this rat model [16]. These characteristics make crosses between F344 and GK rats well suited for identifying genes related to skeletal fracture through pathways shared with type-2 diabetes.

Type-2 diabetes has an impact on bone through several mechanisms with contradictory effects depending on the stage of disease. Hyperinsulinemia may promote bone formation while low levels of insulin, associated with the progression of type-2 diabetes, may cause reductions in BMD [17]. Hyperglycemia is thought to influence bone abnormalities in diabetes by suppressing osteoblast differentiation and proliferation [18, 19]. Several QTLs affecting diabetes-related phenotypes have previously been identified in F2 intercrosses using the GK rat. Especially since QTLs in crosses between GK and F344 have been used to identify and characterize diabetes QTLs, this particular strain combination is ideal for investigations into common genetic mechanisms in type-2 diabetes and osteoporosis-associated phenotypes [15, 20-22].

Recent studies identified mitochondrial influence on type-2 diabetes associated phenotypes by the use of conplastic strains, differing only in their mitochondrial genomes [23]. Another strategy to study mitochondrial interactions is reciprocal crossing of two inbred strains [15]. This results in two F2 populations with divergent mitochondrial DNA (mtDNA), since offspring inherit only maternal mitochondria. In F2 populations, additional factors such as imprinting and QTLs on sex chromosomes must be considered when interpreting reciprocal effects. Data from our lab, based on a reciprocal F2 cross between GK and F344 rats, supports reciprocal interaction effects on diabetes phenotypes (H-B Park et al, unpublished). Additionally, we previously reported that QTLs for trabecular and cortical tibial bone phenotypes measured by pQCT in (GK×F344) F2 crosses with divergent mtDNA are influenced by gender and reciprocal cross [24]. The more than 100 variant positions between GK and F344 mtDNA, including twelve non-synonymous amino acid changes in proteins required for ATP synthesis [25], support the involvement of mtDNA variants as a major factor behind the reciprocal cross effect.

Bone size has a strong impact on bone strength and fracture in humans [26]. In this study, we have characterised three generations (parental, F1 and F2) of the GK and F344 rat strains for bone size phenotypes measured by a new three-dimensional computed tomography (3DCT) method that offers more flexible options in selecting specific regions for analysis compared to pQCT. The general requirements of a computed tomography unit to produce high quality 3D images required for a study such as ours include a high and preferably isotropic spatial resolution and a high signal-to-noise ratio. Many modern clinical CT scanners can achieve this due to their high X-ray output, their very small detector dimensions, their ability to do helical and overlapping sampling, and the possibility to reconstruct thin slices separated by only a fraction of a millimeter. The 3DCT method provide phenotypes associated with skeletal strength to be used in studies of the complex genetic contribution to bone fragility, yet the advantages of this application has not been previously exploited in animal studies.

The aims of this study were: 1) identify QTLs for bone size phenotypes and investigate the effects of sex and reciprocal cross in an F2 intercross between GK and F344, 2) characterise parental and F1 progeny of the GK and F344 rat strains for bone size phenotypes for a better estimation of the genetic effects and future breeding of congenics, 3) evaluate the use and reproducibility of the 3DCT method in small animal bones and 4) investigate if any QTLs are uniquely identified by 3DCT and thereby providing complementary information about bone architecture.

## **Material and Methods**

### **Animals**

Males and females from the diabetic GK (GK/KyoSwe) and non-diabetic F344 (F344/DuCr1Swe) rat strains were included in the study, representing parental strains (GK n=19, F344 n=20), F1 progeny with both reciprocal crosses (n=37) and an F2 population (n=206). Briefly, two separate F2 intercrosses were generated: one originating from grandmaternal GK and grandpaternal F344 (cross 1, (GK female × F344 male) F1), and the other from grandmaternal F344 and grandpaternal GK (cross 2, (F344 female × GK male) F1). The two groups of reciprocal F1 progeny were mated separately to yield two reciprocal F2-populations. From a genetic standpoint, the reciprocal crosses differ by their mitochondrial genotypes as inherited from the founding female. All cross 1 progeny carry GK mitochondrial genotype, males carry the Y-chromosome from F344 and females can only be homozygous for GK-alleles on chr X. Inversely, all cross 2 progeny carry F344 mitochondrial genotype, males carry the Y-chromosome from GK and females can only be homozygous for F344-alleles on chr X.

All rats had free access to tap water and standard commercial rodent chow (R3 from Lantmännen AB, Sweden), containing, in percent of raw nutritional value (1260 Kcal per 100g, 21% protein and 5% fat. Ca and P constituted 1.1% and 0.8% of the minerals. They were kept in the same room with controlled temperature and humidity and a 12 h light/dark cycle with the same number of rats per cage. To mimic the development of ailments in humans associated with the consumption of a high fat diet, all rats were fed a modified fat enriched diet (the same commercial rodent chow supplemented with 2% cholesterol, 20% olive oil, and 0.5% bile acid, Lactamin AB, Linköping, Sweden) starting at the age of 4 months. After completing 90 days of fat enriched diet, the rats were sacrificed at a mean age of  $218 \pm 9$  days. For skeletal phenotypes, left femur and tibia from the parental- and F1 progeny and left tibia from the F2 progeny were collected. The bones were dissected free of fat and muscle, placed in 70% ethanol and stored at room temperature. Genomic DNA was purified from rat liver using QIAmp DNA mini kit (QIAGEN, Valencia, CA, USA). Permit was obtained from the local Animal Ethics Committee.

### **Three-dimensional computed tomography (3DCT)**

Left tibia from all rats were scanned in a CT unit (Somatom Sensation 64, Siemens Ag, Erlangen, Germany). The tibial bones were placed in 70% ethanol in 15 mm diameter plastic

tubes in order to eliminate image reconstruction artefacts that occur if the samples are placed free in air. Images were acquired using 120 kV and 140 mAs per revolution with collimation  $12 \cdot 0.6$  mm and pitch 0.8. The field of view was reduced to 50 mm for maximum geometric resolution. Images with a slice width of 2 mm were reconstructed using reconstruction kernel “u80u” with a reconstruction increment of 0.4 mm. The images produced with the CT scanner therefore represent a 3D voxel matrix with a resolution of  $0.1 \cdot 0.1 \cdot 0.4$  mm.

The images were processed using the Analyze (version 5.0) software package (Biomedical Imaging Resource, Rochester, MN, USA). The 3D voxel matrix was resampled using interpolation to an isotropic resolution of  $0.1 \cdot 0.1 \cdot 0.1$  mm. The bone samples were extracted from the 3D matrix with a volume rendering procedure using Hounsfield value thresholds for extracting either all (cortical and trabecular) bone tissue or only the cortical regions.

The following measurements were made on the bones: Total and cortical bone volume ( $\text{mm}^3$ ), cortical bone volume fraction (%), total and cortical mean Hounsfield number, straight and curved length (mm) and peri- and endosteal area at mid-shaft ( $\text{mm}^2$ ). Peri- and endosteal area at fibula-site ( $\text{mm}^2$ ) was also measured, primarily because in these small bones it was a distinct site and likely to correspond to the transition between metaphyseal and diaphyseal bone (Fig. 1).

The volumetric BMD (vBMD) ( $\text{mg}/\text{cm}^3$ ) was calculated using a calibration method previously developed for determining bone mass in human vertebrae [27]. Since the calibration of the CT unit is dependent on the size of the scanned object, the calibration equation was re-calculated to ensure validity for the very small objects used in this study. This was performed by scanning the BMD calibration standards in the same geometry as the bone samples, allowing total and cortical measured vBMD ( $\text{mg}/\text{cm}^3$ ) to be calculated from the respective mean Hounsfield value measurements.

### *Reproducibility of 3DCT analysis*

The reproducibility of the analytical procedure was tested by repeating the analysis of the first scan using the same rats ( $n=40$ ) to calculate intra-observer CV for each analyzed parameter. A second scan at a different time point from the initial measurement was performed, repeating the measurements of the left tibia from 5 male and 5 female rats of each strain and cross ( $n=40$ ). The duplicate scans and the subsequent analysis were made by the same operator (SL). Additionally, we evaluated if the method was equally reliable in high and low size intervals by analyzing ten rats of varying body size for periosteal mid-tibial circumference in order to calculate the correlation with previous mid-tibial area measurement.

### *Accuracy of 3DCT analysis*

For the purpose of determining the accuracy of the CT method for volume determination, objects with known volumes were scanned, using the same scanning parameters as for the rat bones. The objects consisted of plexiglass rods with carefully measured dimensions. The diameter and length of the objects were measured with a digital sliding caliper (Mauser, Digital 6, 8M007906, Switzerland) which in its turn was calibrated against a calibration object (series 167-102, Mitutoyo Corp., Kawasaki, Japan) with a length of  $50 \pm 0.002$  mm. The plexiglass rods had volumes of 180.27, 320.47 and 494.81 mm<sup>3</sup>, respectively, when measured with the caliper. The corresponding values when measured with the 3DCT method were 179.6, 319.7 and 494.5 mm<sup>3</sup>, respectively.

### Statistical analysis

All phenotypes were normally distributed or log-transformed to a normal distribution. To compare the bone size phenotypes between males and females and between the reciprocal crosses, one-way ANOVA was used. The level of significance was set at  $p < 0.05$ . Unless stated,  $p$ -values are nominal. Phenotypes were adjusted for cross, age, litter size, and body-weight using regression analysis. Residuals were saved and used in the QTL analysis. To account for differences between sexes, the residuals were computed separately for each sex.

### Genotyping and linkage analysis of quantitative traits

The proportion of genetic variance responsible for the 3DCT traits was calculated as percentage of genetic variance =  $1 - (\text{variance of F1} / \text{variance of F2})$ . A total of 192 genome-wide microsatellite markers were genotyped and a genetic linkage map was generated as described previously [24]. Genetic linkage analysis was performed for each sex separately. In order to identify possible interaction differences between loci in the nuclear genome and reciprocal cross, the sex separated F2 progeny were additionally separated on the basis of reciprocal cross. QTLs on autosomes were identified employing MAP MANAGER/QTX v. b20 [28]. The X chromosome was analysed using R/qtl [29]. Mapping QTLs on the X chromosome was conducted for each sex separately without further separation by cross. Permutation tests were performed to establish genome-wide significance levels by randomization of the phenotypic data in relation to genotypic data [30]. Significant (i.e., genome-wide false-positive rate below 5%) and suggestive (i.e., genome-wide false-positive rate of 63%) linkage was employed to establish genome-wide thresholds [31, 32]. The

likelihood ratio statistic (LRS) for significant linkage range 17.6-18.2 (LOD=3.8-3.9) and for suggestive linkage LRS range 10.7-11.2 (LOD=2.3-2.4).

### Evaluation of sex- and reciprocal cross-specific QTLs

Sex- and reciprocal cross-specific QTLs were identified using the method described previously [24]. To identify sex specific QTLs, the LOD score differences between males and females across the genome were assessed ( $\Delta\text{LOD}_{\text{sex}}$  score). We applied a permutation method to evaluate sex specific QTLs, where thresholds were established using two randomly selected equal sized subsets of males and females [33]. The randomization was conducted within each cross. Bone phenotypes in the two subsets were then permuted to calculate  $\Delta\text{LOD}_{\text{sex}}$  scores across the genome. Genetic markers on the X chromosome were not included in these permutation tests. The average  $\Delta\text{LOD}_{\text{sex}}$  score for genome-wide significant sex-specificity at suggestive ( $\alpha = 0.63$ ) and significant ( $\alpha = 0.05$ ) levels were 2.3 and 3.7, respectively.

Within each sex, subsequent reciprocal cross-separated linkage analyses were conducted to identify cross specific QTLs. The LOD score differences between cross 1 and cross 2 ( $\Delta\text{LOD}_{\text{cross}}$  score) across the genome were examined. Thresholds of the cross specific QTL were computed by permutation using two randomly selected equal sized cross 1 and cross 2 subsets. The average  $\Delta\text{LOD}_{\text{cross}}$  score for genome-wide significant cross-specificity at suggestive ( $\alpha = 0.63$ ) and significant ( $\alpha = 0.05$ ) level were 2.4 and 3.9, respectively.

To confirm the sex- and cross-specific QTLs identified with the  $\Delta\text{LOD}$  method, likelihood ratio tests were performed comparing a full model with a QTL $\times$ sex or cross interaction term and a reduced model without the interaction term, using both male and female data for the sex interaction and each sex separately for cross interaction. Residuals of each phenotype were examined for normality using normal probability plots. The level of significance for a specific QTL interaction with sex or cross was set at  $p < 0.05$ .

A statistical power calculation using the method of Lynch and Walsh et al [34] was conducted as described previously [24]. Using a LOD score of 2.4 to control false positive detection of linkage, a sample size of 52 is necessary to achieve 80% statistical power for detecting a QTL with  $R^2$  value of 0.25.

## **Results**

### *Precision of 3DCT*

Evaluation of the 3DCT method showed overall very low parameter dependent variability in repeated scans, with CV's ranging from 0-8.2% (Supplementary Table 1). Intra-observer analysis yielded variations between 0.4-9.2%.

### *Phenotypic analyses of the parental strains, F1- and F2-generations*

The 3DCT results for male GK and F344 rats demonstrated overall larger tibial bone size variables, with the exception of bone length, in the GK males (Table 1A). In females, the differences pointed in the same direction (Table 1B). The phenotype distribution of total tibial bone volume in the parental, F1 and F2 generations is shown in (Fig. 2). There was a more pronounced difference in total tibial bone volume between GK and F344 females as compared to males. The female F1 progeny showed an intermediate phenotypic value, while the male F1 progeny exhibited a more GK-like phenotype. For both sexes, the F2 generation displayed a more variable phenotype, reflecting the effect of genetic heterogeneity.

The 3DCT phenotypes for tibia in F1 males were similar in the two reciprocal crosses (Table 1A). In female F1 rats, the findings were similar with the exception of the curved tibia length, which was significantly higher (+6.7%,  $p=0.009$ ) in the cross with GK maternal origin (Table 1B).

In the F2 progeny, strong sexual dimorphism was observed for all traits (Table 2). All CT traits were significantly higher in males. Phenotypic differences were also observed between F2 progeny from the two reciprocal crosses, with more pronounced differences in female rats. In males, cortical volume was 3% higher ( $p=0.02$ ) in progeny with GK grandmaternal origin (Table 2). In female rats a larger number of phenotypes differed depending on the reciprocal cross: total and cortical volume, cortical bone volume fraction, straight length and cortical midshaft CSA values were all higher in progeny with GK grandmaternal origin ( $p$ -values 0.02-0.009, Table 2). For total bone volume, the proportion attributable to genetic variance was 42% in males and 78% in females.

### *QTLs in males and females*

The genome-wide significant QTLs identified in males are summarized in (Table 3A). Three QTLs attained genome-wide significance in all males; a locus on chr 1 (51-67 cM) where two phenotypes mapped (PAmid, LOD 3.8 and EAFib, a locus in chr 9 (67-82 cM) for EAFib (LOD 6.7), and a locus on chr 10 (75-84 cM) for PAmid (LOD 4.0). Evaluation of  $\Delta\text{LOD}_{\text{sex}}$

demonstrated that three of the QTLs were male specific ( $\Delta\text{LOD}_{\text{sex}} > 2.3$ ), and significant male-specific interaction was confirmed for the QTL for EAfib (endosteal area at the fibula-site) on chr 9 (LR =19,  $p=0.0001$ ) in the likelihood ratio tests.

The genome-wide significant QTLs identified in females are summarized in (Table 3B). Three genome-wide significant QTLs were identified in all females; a locus on chr 1 (39-64 cM, LOD=3.8) for EAfib, and two separate QTLs on chr 3 (0-14 cM and 20-33 cM) for PAfib and total vBMD (LOD 4.4 and 4.3). Two QTLs identified in females reached genome-wide significance with  $\Delta\text{LOD}_{\text{sex}}$  evaluation ( $\Delta\text{LOD}_{\text{sex}} > 2.3$ ), but none reached significance for female-specific interaction in the likelihood ratio tests.

### *Reciprocal cross-separated QTL analysis in males and females*

The reciprocal cross-separated QTL analysis for each sex allowed identification of additional significant QTLs and generated further support for several loci already identified in all F2 animals of each sex (Table 3A and 3B).

A new genome-wide significant QTL (43-79 cM) for the cortical bone volume fraction (LOD 4.4) was mapped on chr 17 in F2 males from cross 1 and three loci in cross 2 males: total bone volume on chr 6 (31-50 cM, LOD 3.8), cortical bone volume on chr 8 (42-62 cM, LOD 3.8) and cortical area at the fibula site on chr 14 (72-84 cM, LOD 3.9). The new QTL on chr 14 was different between the two crosses with  $\Delta\text{LOD}_{\text{cross}}$  evaluation ( $\Delta\text{LOD}_{\text{cross}} > 2.4$ ), but the interaction term was not significant in the likelihood ratio test. The locus on chr 1 mapped earlier in all males was convincingly confirmed in cross 1 (LOD 4.1 and 7.2) for the two phenotypes mapping to the locus.

In cross-separated females, a new genome-wide significant QTL was identified on chr 4 (36-48 cM) for cortical and total bone volume in cross 1 (LOD 4.9 and 5.6) (Table 1B). This QTL was different between the reciprocal crosses (genome-wide significant,  $\Delta\text{LOD}_{\text{cross}} > 3.9$ ) and had a highly significant interaction term (between reciprocal cross and QTL) in the likelihood ratio test ( $p=0.002$ ). One of the earlier identified QTLs on chr 3 (0-14 cM, PAfib, Table 1B) in female progeny was also different between crosses and highly significant for the interaction term ( $p=0.005$ ). The two cross specific QTLs were only detected in progeny of GK grandmaternal origin (cross) and were not found in the aggregated analysis with females from both reciprocal crosses (Fig. 3).

Additionally, genome-wide suggestive linkage (LOD > 2.3) to several bone size phenotypes were detected in both males and females. In males, ten QTLs on chr 1, 2, 3, 6, 8, 10, 12, 14,

16 and 17 were identified and in females, twelve QTLs were found on chr 1, 2, 3, 4, 7, 8, 10 and 14 (data not shown). Suggestive linkage was also detected in the reciprocal cross-separated QTL analysis for each sex. In males with GK grandmaternal origin, four QTLs were detected on chr 2, 3, 5 and 20 and three QTLs were identified on chr 5, 6 and 18 in the cross with F344 grandmaternal origin. In females with grandmaternal origin, a suggestive QTL was detected on chr 3 (data not shown).

The GK allele had an increasing effect on genotypic mean values for all QTLs in both sexes.

## ***Discussion***

In this study, we identified QTLs for bone size phenotypes with sex- and reciprocal cross specific interactions. The observed interaction between nuclear QTLs and cross provides additional evidence for its effect on bone traits [24]. Several QTLs overlapped our previously identified QTLs for pQCT phenotypes using the same F2 rats [24], but we also identified new QTLs determined with this application of the 3DCT method. The QTLs on chr 4 and 6, are uniquely identified by the 3DCT and not shared with any QTL generated by pQCT. These findings illustrate the complexity of the genetic architecture of bone, and that dimension properties such as circumference and length are only partially related, clearly illustrating the importance of complementary methods for bone analysis. In humans, genome-wide scans are beginning to yield important information on specific candidate genes for osteoporosis, while animal models contribute to the knowledge of other aspects of bone, especially candidate genes for overall size effects.

In line with the reports on an association between anabolic effects of type-2 diabetes and bone in human populations [35], the bone size parameters showed predominantly higher values in the diabetic GK rat compared to the non-diabetic F344 rat. GK alleles associated in all instances with higher genotypic means substantiate this observation.

Linkage analysis in the F2 population identified significant QTLs for bone size on chr 1, 9 and 10 in all males and on chr 1 and 3 in all females. Male-specific interaction was demonstrated for the QTL on chr 9 linked to endosteal area at the fibula-site (EAFib). Chromosome 1 (39-67 cM) contained a number of QTLs linked to several bone size parameters in both males and females in the (GK×F344)F2 progeny. These overlapped our previously reported pQCT QTLs linked to tibial cross-sectional area (CSA), bone mineral content (BMC), moment of inertia (IP) and resistance (RP), periosteal- (PC) and endosteal (EC) circumference [24]. The same region also overlaps QTLs for fasting glucose [15, 20], establishing this region as a candidate region for genetic fine mapping to elucidate possible mechanisms between type-2 diabetes and bone size. Adding to the evidence that this is an important region in bone regulation, it also overlaps with QTLs linked to areal BMD and cortical area of femur identified in a (F344×LEW)F2 rat cross [6, 13]. Of note, this chr 1 locus harbours the osteoporosis candidate genes transforming growth factor beta 1 (TGFB1) and estrogen receptor alpha (ESR1) [36, 37].

The reciprocal cross-separated QTL analysis identified a cross-specific QTL on chr 4 for cortical and total bone volume that was only detected in females from the cross carrying

mtDNA from GK. Since linkage was only detected in rats with GK mtDNA, it is interesting to note that three nuclear genes encoding mitochondrial proteins are located within this QTL: the mitochondrial ribosomal protein [Mrps33], the NADH dehydrogenase (ubiquinone) 1 beta subcomplex 2 [Ndufb2] and glutathione S-transferase kappa 1 [Gstk1]. Furthermore, this region overlaps a previously identified QTL strongly linked to femoral neck structure phenotypes in (F344×LEW)F2 rats [13]; and a gene expression study identified several candidate genes within this QTL, which are involved in bone metabolism (IGF2, FGF2, VEGF, TNF) and correlated with the investigated phenotypes [38]. This chromosome region is also homologous to a region in the human genome where linkage to femoral neck related phenotypes has been identified [39-42].

In males, suggestive cross-specific interaction was identified on chr 14 (cortical area at the fibula-site) for cross 2 carrying F344 mtDNA. This QTL was not detected in the aggregated analysis of all males, suggesting that unique interactions among nuclear genes and the two types of mtDNA occur and that it influences bone size phenotypes at significant levels. This result provides additional support for our previous identification of several reciprocal cross-specific QTLs linked to pQCT traits [24]. In this study, no significant QTLs were detected on the X-chromosome, but we cannot exclude the possibility that a Y-chromosome linked QTL could contribute to the observed reciprocal cross effect for the identified QTL on chr 14 in males. Genomic imprinting could be a possible explanation to the observed reciprocal effect due to its parent-of-origin specific inheritance. However, the more than 100 variant positions that have been identified in GK mtDNA compared to F344 [25], support the involvement of mtDNA as a major factor behind the observed reciprocal cross effect.

To further delineate the factors underlying the complex genetic architecture of bone phenotypes, analysis of epistatic effects between the various genetic loci that contribute to fracture risk could be employed. However, such analysis requires considerably larger sample sizes.

Since we analyzed each bone trait separately, the correlation between phenotypes and overlapping QTLs needs to be considered. Closely correlated phenotypes (i.e. total and cortical volume, periosteal and endosteal area, cortical and total vBMD with correlation coefficients ranging from 0.79-0.91) showed overall linkage to the same chromosomal regions, but this is not evidence for common underlying genetic mechanisms. The same region could include tightly linked genes that influence the correlated phenotypes independently. To elucidate the presence of several adjacent QTLs, compared to a single QTL affecting multiple phenotypes, additional studies are required. Such studies could include

strategies to increase the genetic resolution e.g. by increasing the sample, increasing the number of intercross generations (generating advanced intercross lines) or breeding of small congenics. Another approach could be the inclusion of data from additional rat strains and intercrosses in order to separate independent phenotypes.

Compared to already available imaging technologies of bone in experimental animals such as DXA, pQCT, micro-CT and biomechanical testing [43-48] the described 3DCT method provides additional valuable information about bone size characteristics of both the entire- and cortical bone. Using a dedicated small object CT scanner, such as the Stratec XCT 2000, was considered but was eventually abandoned since it is only capable of scanning in a sequential mode, which makes the movement of the object between scans critical to 3D image quality in geometrical terms. Additionally, the output of the X-ray tube is extremely low and results in noise in the reconstructed images that seriously impairs 3D image quality. The 3DCT method shows high precision with exceptionally low intra- and inter-analysis CV's for all measured parameters (<1.5%) except for those related to the inner contour (endosteal circumference) of tibia, possibly explained by the small size and low pixilation. This application of the 3DCT analysis also has the advantage of being high throughput (less than 1 minute per set of 5 bones scanned). We therefore regard the 3DCT method as an important new tool to assess bone size in animal models.

In humans, bone size changes very little after having reached adulthood while by contrast, there is an age-related decline in bone mineral density. The rat model measured at 218 days (equivalent to 'middle-age'), mirrors the adult state and therefore the QTLs identified most likely represent a mature state in bone development rather than genes contributing to age-related degeneration. Verification of potential bone fragility QTLs may have been possible by performing a detailed analysis of the distribution and content of trabecular bone in the metaphyseal area, since this region has been shown to be abnormal in diabetes. A weakness of our study is that this was not done and is no longer possible since the bones have been destroyed in subsequent experiments.

In summary, this study shows that the phenotypic manifestations of bone size as well as its genetic regulation are influenced both by sex and reciprocal cross. The 3DCT method allows detailed characterisation of bone size variables, where linkage to the QTL regions on chr 1 and chr 4 are of particular interest; the region on chr 1 overlaps with loci for type 2 diabetes and energy homeostasis; and the region on chr 4 appear to map to size determinants not only in tibia but also in femur. The observed interaction between nuclear QTLs regulating bone size and reciprocal cross motivates further investigation of mitochondrial effects on bone.

**Table 1A.** 3DCT results of tibia in male rats.

	GK	F344	Percentage diff. (p-value)	GKxF344 F1	F344xGK F1	Percentage diff. (p-value)
Number of rats	9	10		8	9	
Age (days)	231 (227-235)	229 (225-233)	NS	216 (212-233)	233 (226-239)	0.0003
<b>Bone size (Tibia)</b>						
Total bone volume (TotBV) (mm <sup>3</sup> )	462 ± 31	404 ± 30	14 (0.0007)	502 ± 24	490 ± 47	2.4 (NS)
Cortical bone volume (CortBV) (mm <sup>3</sup> )	190 ± 16	165 ± 8.8	15 (0.0006)	206 ± 13	208 ± 16	1.0 (NS)
Cortical bone volume fraction (%)	41.0 ± 0.9	41.0 ± 3.0	~0 (NS)	41.0 ± 1.0	43.0 ± 3	-2.0 (NS)
Length (straight) (mm)	44.3 ± 1.3	44.1 ± 1.4	0.5 (NS)	45.8 ± 1.1	45.0 ± 1.6	1.8 (NS)
Length (curved) (mm)	52.6 ± 3.7	50.0 ± 1.9	5.2 (NS)	53.4 ± 1.7	51.9 ± 4.7	2.9 (NS)
Cortical midshaft PA (PAmid) (mm <sup>2</sup> )	11.3 ± 0.8	8.1 ± 0.6	40 (<10 <sup>-4</sup> )	10.6 ± 0.2	10.7 ± 0.6	-0.9 (NS)
Cortical midshaft EA (EAmid) (mm <sup>2</sup> )	3.8 ± 0.2	2.0 ± 0.2	90 (<10 <sup>-4</sup> )	3.2 ± 0.2	3.2 ± 0.3	~0 (NS)
Cortical midshaft CSA (mm <sup>2</sup> )	7.5 ± 0.6	6.0 ± 0.2	25 (<10 <sup>-4</sup> )	7.3 ± 0.3	7.5 ± 0.6	-2.7 (NS)
Cortical fibula PA (PAfib) (mm <sup>2</sup> )	10.6 ± 1.0	7.5 ± 0.8	41 (<10 <sup>-4</sup> )	10.4 ± 0.7	10.4 ± 1.1	~0 (NS)
Cortical fibula EA (EAfib) (mm <sup>2</sup> )	2.4 ± 0.2	1.3 ± 0.1	85 (<10 <sup>-4</sup> )	2.0 ± 0.2	2.2 ± 0.2	-9.1 (0.03)
Cortical fibula CSA (mm <sup>2</sup> )	8.1 ± 1.0	6.2 ± 0.8	31 (0.0003)	8.4 ± 0.6	8.1 ± 1.0	3.7 (NS)
<b>Bone mineral density</b>						
Total vBMD (mg/cm <sup>3</sup> )	1322 ± 10	1335 ± 26	-1.0 (NS)	1338 ± 16	1356 ± 26	-1.3 (NS)
Cortical vBMD (mg/cm <sup>3</sup> )	1848 ± 10	1822 ± 12	1.4 (<10 <sup>-4</sup> )	1851 ± 14	1857 ± 5.0	-0.3 (NS)

**Table 1B.** 3DCT results of tibia in female rats.

	GK	F344	Percentage diff. (p-value)	GKxF344 F1	F344xGK F1	Percentage diff. (p-value)
Number of rats	10	10		10	10	
Age (days)	228 (220-235)	231 (230-233)	NS	212 (209-214)	236 (231-239)	(<10 <sup>-4</sup> )
<b>Bone size (Tibia)</b>						
Total bone volume (TotBV) (mm <sup>3</sup> )	371 ± 19	285 ± 14	30 (<10 <sup>-4</sup> )	327 ± 12	329 ± 20	-0.6 (NS)
Cortical bone volume (CortBV) (mm <sup>3</sup> )	158 ± 11	105 ± 6.7	50 (<10 <sup>-4</sup> )	125 ± 4.2	128 ± 11	-2.3 (NS)
Cortical bone volume fraction (%)	43.0 ± 1.0	37.0 ± 1.0	6.0 (<10 <sup>-4</sup> )	38.0 ± 1.0	39.0 ± 1.0	-1.0 (NS)
Length (straight) (mm)	39.7 ± 1.1	38.4 ± 1.2	3.4 (0.02)	40.0 ± 0.8	39.7 ± 1.0	0.8 (NS)
Length (curved) (mm)	46.1 ± 3.5	45.2 ± 2.3	2.0 (NS)	48.0 ± 1.9	45.0 ± 2.5	6.7 (0.009)
Cortical midshaft PA (PAmid) (mm <sup>2</sup> )	9.4 ± 0.5	6.1 ± 0.3	54 (<10 <sup>-4</sup> )	7.5 ± 0.4	7.7 ± 0.5	-2.6 (NS)
Cortical midshaft EA (EAmid) (mm <sup>2</sup> )	2.9 ± 0.1	1.2 ± 0.1	142 (<10 <sup>-4</sup> )	2.0 ± 0.1	1.9 ± 0.1	5.2 (NS)
Cortical midshaft CSA (mm <sup>2</sup> )	6.6 ± 0.5	4.9 ± 0.3	35 (<10 <sup>-4</sup> )	5.6 ± 0.4	5.8 ± 0.4	-3.4 (NS)
Cortical fibula PA (PAfib) (mm <sup>2</sup> )	9.7 ± 0.9	6.3 ± 0.7	54 (<10 <sup>-4</sup> )	7.5 ± 0.5	7.7 ± 0.6	-2.6 (NS)
Cortical fibula EA (EAfib) (mm <sup>2</sup> )	2.1 ± 0.1	0.9 ± 0.09	133 (<10 <sup>-4</sup> )	1.4 ± 0.1	1.5 ± 0.1	-6.7 (NS)
Cortical fibula CSA (mm <sup>2</sup> )	7.6 ± 0.8	5.4 ± 0.8	41 (<10 <sup>-4</sup> )	6.1 ± 0.5	6.3 ± 0.6	-3.2 (NS)
<b>Bone mineral density</b>						
Total vBMD (mg/cm <sup>3</sup> )	1341 ± 6	1281 ± 11	4.7 (<10 <sup>-4</sup> )	1299 ± 10	1305 ± 17	-0.5 (NS)
Cortical vBMD (mg/cm <sup>3</sup> )	1819 ± 16	1795 ± 25	1.3 (0.02)	1799 ± 10	1798 ± 18	0.06 (NS)

Phenotypes are presented as mean ± sd. PA = periosteal area; EA = endosteal area; CSA = cross-sectional area; vBMD = volumetric bone mineral density, CortBV/TotBV = cortical bone volume fraction

**Table 2.** 3DCT results for tibia. Sex and reciprocal cross effects in F2 males and females.

	Sex effects			Reciprocal Cross Effects					
	Females		Males	Females			Males		
	Irrespective of cross		Percentage diff. (p-value)	Cross 1 GKxF344	Cross 2 F344xGK	Percentage diff. (p-value)	Cross 1 GKxF344	Cross 2 F344xGK	Percentage diff. (p-value)
Number of rats	98	108		48	50		66	42	
Age (days)	215 (204-232)	215 (206-233)		215 (204-232)	215 (201-225)		216 (207-233)	214 (206-231)	
Body weight (g)	248±27	426±44	-42 (<10 <sup>-4</sup> )	247±25	248±28	-0.4 (NS)	423±44	423±45	+0.05 (NS)
<b>Bone size</b>									
Total bone volume (TotBV) (mm <sup>3</sup> )	323 ± 34	418 ± 50	-23 (<10 <sup>-4</sup> )	329 ± 31	316 ± 36	+3.7 (0.04)	420 ± 52	415 ± 47	+1.1 (NS)
Cortical bone volume (CortBV) (mm <sup>3</sup> )	125 ± 16	184 ± 20	-32 (<10 <sup>-4</sup> )	128 ± 15	121 ± 16	+5.9 (0.009)	186 ± 21	181 ± 19	+2.3 (0.02)
Cortical bone volume fraction (%)	0.39 ± 0.02	0.44 ± 0.02	-11 (<10 <sup>-4</sup> )	0.39 ± 0.02	0.38 ± 0.02	+2.6 (0.02)	0.44 ± 0.02	0.44 ± 0.02	~0 (NS)
Length (straight) (mm)	39.7 ± 1.4	44.5 ± 1.7	-11 (<10 <sup>-4</sup> )	40.0 ± 1.3	39.5 ± 1.5	+1.3 (0.04)	44.5 ± 1.9	44.5 ± 1.5	~0 (NS)
Length (curved) (mm)	45.0 ± 2.3	50.2 ± 2.4	-10 (<10 <sup>-4</sup> )	45.3 ± 2.4	44.7 ± 2.1	+1.3 (NS)	50.2 ± 2.5	50.2 ± 2.4	~0 (NS)
Cortical midshaft PA (PAmid) (mm <sup>2</sup> )	7.2 ± 0.7	9.4 ± 1.0	-23 (<10 <sup>-4</sup> )	7.2 ± 0.7	7.2 ± 0.7	~0 (NS)	9.4 ± 1.1	9.5 ± 1.0	-1.1 (NS)
Cortical midshaft EA (EAmid) (mm <sup>2</sup> )	1.7 ± 0.3	2.7 ± 0.5	-37 (<10 <sup>-4</sup> )	1.7 ± 0.3	1.7 ± 0.3	~0 (NS)	2.6 ± 0.5	2.8 ± 0.5	-7.1 (NS)
Cortical midshaft CSA (mm <sup>2</sup> )	5.5 ± 0.5	6.8 ± 0.7	-19 (<10 <sup>-4</sup> )	5.5 ± 0.6	5.4 ± 0.5	+2.2 (0.05)	6.8 ± 0.7	6.7 ± 0.6	+0.9 (NS)
Cortical fibula PA (PAfib) (mm <sup>2</sup> )	7.2 ± 0.6	8.5 ± 1.0	-15 (<10 <sup>-4</sup> )	7.2 ± 0.7	7.2 ± 0.6	~0 (NS)	8.5 ± 1.0	8.6 ± 1.0	-1.1 (NS)
Cortical fibula EA (EAfib) (mm <sup>2</sup> )	1.5 ± 0.3	2.0 ± 0.4	-25 (<10 <sup>-4</sup> )	1.4 ± 0.3	1.5 ± 0.3	-6.7 (NS)	2.0 ± 0.4	2.1 ± 0.4	-4.8 (NS)
Cortical fibula CSA (mm <sup>2</sup> )	5.7 ± 0.6	6.5 ± 0.8	-12 (<10 <sup>-4</sup> )	5.7 ± 0.7	5.7 ± 0.5	+1.2 (NS)	6.5 ± 0.8	6.5 ± 0.8	-0.6 (NS)
<b>Bone mineral density</b>									
Total vBMD (mg/cm <sup>3</sup> )	1304 ± 26	1400 ± 43	-6.9 (<10 <sup>-4</sup> )	1309 ± 25	1299 ± 26	+0.8 (NS)	1407 ± 43	1391 ± 43	+1.1 (NS)
Cortical vBMD (mg/cm <sup>3</sup> )	1821 ± 15	1870 ± 19	-2.6 (<10 <sup>-4</sup> )	1821 ± 15	1822 ± 19	-0.05 (NS)	1873 ± 20	1865 ± 17	+0.4 (NS)

Phenotypes are presented as mean ± sd. PA = periosteal area; EA = endosteal area; CSA = cross-sectional area; vBMD = volumetric bone mineral density; CortBV/TotBV = cortical bone volume fraction

**Table 3A.** Bone size related QTLs in tibia from male F2 rats

Chr	Position <sup>a</sup> (cM)	Phenotype	LOD score <sup>b</sup>			Sex <sup>c</sup>	Cross <sup>d</sup>
			All N=108	Cross 1 N=66	Cross 2 N=42	LR (p-value)	LR (p-value)
1	D1Rat20-D1Wox16 (51-67)	PAmid	<b>3.8</b>	<b>4.1</b>	1.7		
1	D1Rat20-D1Wox16 (55-67)	EAFib	<b>6.7</b>	<b>7.2</b>	2.5		
6	D6Mgh11-D3Mit19 (31-50)	TotBV	3.4	0.9	<b>3.8</b>		
8	D8Mit2-D8Mgh4 (42-62)	CortBV	3.1	0.7	<b>3.8</b>		
9	D9Mgh2-D9Rat4 (67-82)	EAFib	<b>4.1*</b>	2.9	3.0	19 (0.0001)	
10	D10Mgh5-D10Mgh4 (75-84)	PAmid	<b>4.0</b>	2.5	1.5		
14	D14Mit10-D14Rat22 (72-84)	CAfib	1.3	0.04	<b>3.9*</b>		10.7 (0.005)
17	D17Rat12-D17Mit4 (43-79)	CortBV/TotBV	3.5	<b>4.4</b>	0.2		

<sup>a</sup> The approximate size of the locus was defined as the region covered by a 1-LOD reduction for any of the bone traits.

<sup>b</sup> All QTLs above genome-wide significant threshold (LOD>3.8) detected either in males or in one reciprocal cross are reported in bold.

<sup>c</sup> Male-specific QTLs ( $p<0.05$ ) were validated by likelihood ratio (LR) tests for QTL-by-sex interaction. The LR-test was done only for loci with  $\Delta\text{LOD}>2.3$ .

<sup>d</sup> Reciprocal cross-specific QTLs ( $p<0.05$ ) were validated by likelihood ratio (LR) tests for QTL-by-cross interaction. The LR-test was done only for loci with  $\Delta\text{LOD}>2.4$ .

\*Suggestive male- or reciprocal cross specific QTL interaction ( $p<0.05$ ,  $\Delta\text{LOD}>2.3/\Delta\text{LOD}>2.4$ ).

TotBV = total bone volume; CortBV = cortical bone volume; CortBV/TotBV = cortical bone volume fraction; PAmid = periosteal area at midshaft; EAFib = endosteal area at fibula-site; CAfib = cortical area at fibula-site

**Table 3B.** Bone size related QTLs in tibia from female F2 rats

Chr	Position <sup>a</sup> (cM)	Phenotype	LOD score <sup>b</sup>			Cross <sup>c</sup>
			All N=98	Cross 1 N=48	Cross 2 N=50	LR (p-value)
1	D1Mit9-D1Wox16 (39-64)	EAFib	<b>3.8</b>	2.6	1.0	
3	D3Mit10-D3Rat46 (0-14)	PAfib	<b>4.4</b>	<b>4.8*</b>	1.7	9.7 (0.008)
3	D3Rat189-D3Mit8 (20-33)	TotBMD	<b>4.3</b>	1.5	3.2	
4	D4Mit9-D4Mit24 (37-48)	CortBV	1.1	<b>4.9**</b>	0.1	12.1 (0.002)
4	D4Mit9-D4Mit24 (36-48)	TotBV	1.9	<b>5.6**</b>	0.6	7.9 (0.02)

<sup>a</sup> The approximate size of the locus was defined as the region covered by a 1- LOD reduction for any of the bone traits.

<sup>b</sup> All QTLs above genome-wide significant threshold (LOD=3.8) detected either in females or in one reciprocal cross are reported in bold.

<sup>c</sup> Reciprocal cross-specific QTLs ( $p<0.05$ ) were validated by likelihood ratio (LR) tests for QTL-by-cross interaction. The LR-test was done only for loci with  $\Delta\text{LOD}>2.4$ .

\* Suggestive reciprocal cross-specific QTL interaction ( $p<0.05$ ,  $\Delta\text{LOD}>2.4$ ).

\*\* Significant reciprocal cross-specific QTL interaction ( $p<0.05$ ,  $\Delta\text{LOD}>3.9$ ).

TotBV = total bone volume; CortBV = cortical bone volume; PAfib = periosteal area at fibula-site; EAFib = endosteal area at fibula-site;

TotBMD = total bone mineral density

**Supplementary Table 1.** Coefficients of variation (CV) for repeated tibia 3DCT scans and independent analyses

	Total Bone Volume	Cortical Bone Volume	Total vBMD	Cortical vBMD	Length (Straight)	Length (Curved)	PA mid	EA mid	PA fib	EA fib
<b>Scan<sup>a</sup></b>	0.0	0.0	0.0	0.0	1.8	5.9	2.9	4.5	3.9	8.2
<b>Observer<sup>b</sup></b>	0.9	2.2	0.4	0.6	1.5	5.7	3.3	9.2	4.2	8.4

<sup>a</sup> Represent CV for repeated scan measurements and subsequent analysis in percent.

<sup>b</sup> Represent CV for repeated analysis of the same scan in percent.

vBMD = volumetric bone mineral density; PAmid = periosteal area at midshaft; EAmid = endosteal area at midshaft; PAfib = periosteal area at fibula-site; EAfib = endosteal area at fibula-site

**Fig.1.** Images generated from the 3D CT for determination of the following variables:

The entire bone: (A) Total bone volume ( $\text{mm}^3$ ) and vBMC ( $\text{mg}/\text{cm}^3$ ), (B) Cortical bone volume ( $\text{mm}^3$ ) and vBMC ( $\text{mg}/\text{cm}^3$ ) (trabecular bone subtracted), (C) Total straight and curved length (mm) with fibula (1) and midshaft (2) positions marked.

Transverse view: (D) Periosteal area ( $\text{mm}^2$ ), i.e., the cross-sectional area delineated by the outer circumference and (E) endosteal area ( $\text{mm}^2$ ), i.e., the cross-sectional area delineated by the inner circumference at (C1) mid-shaft and (C2) fibula-site of tibia for both variables.

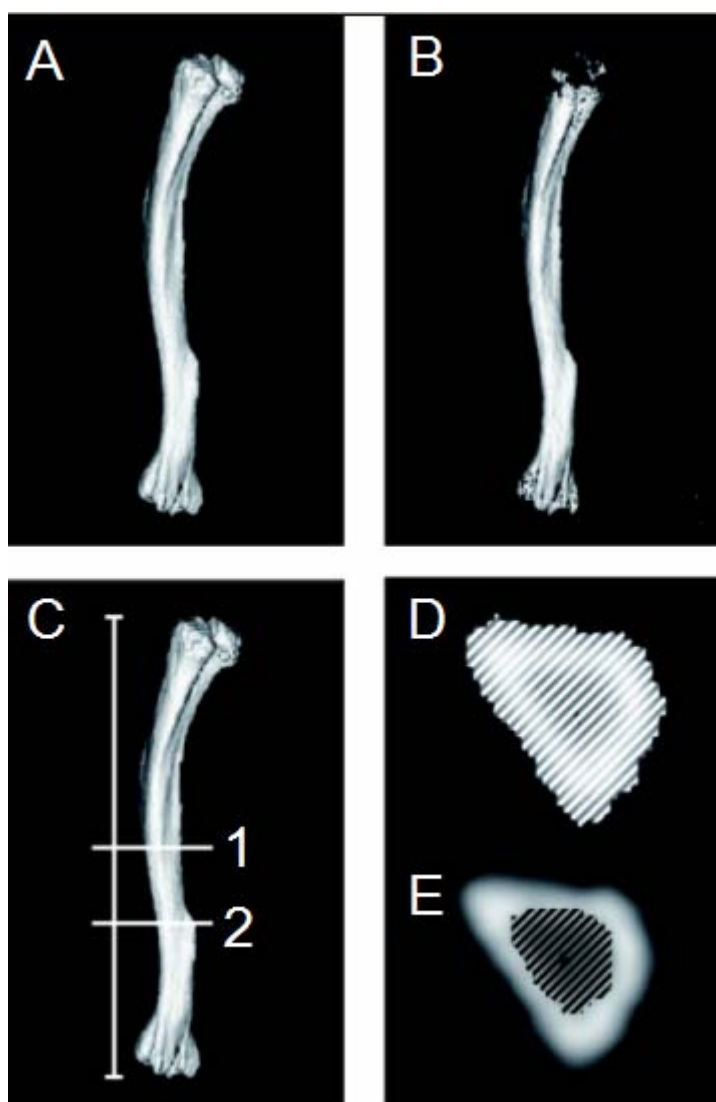


**Fig 2.** Boxplots of total bone volume of tibia. Panels display measurements from parental GK and F344 rats, F1 and F2 rats. Total bone volume in males (A), total bone volume in females (B).

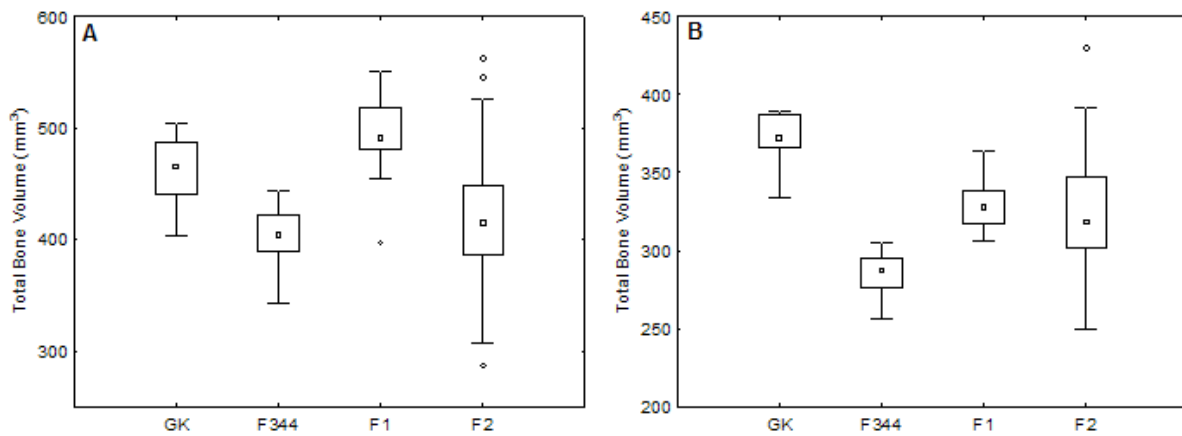
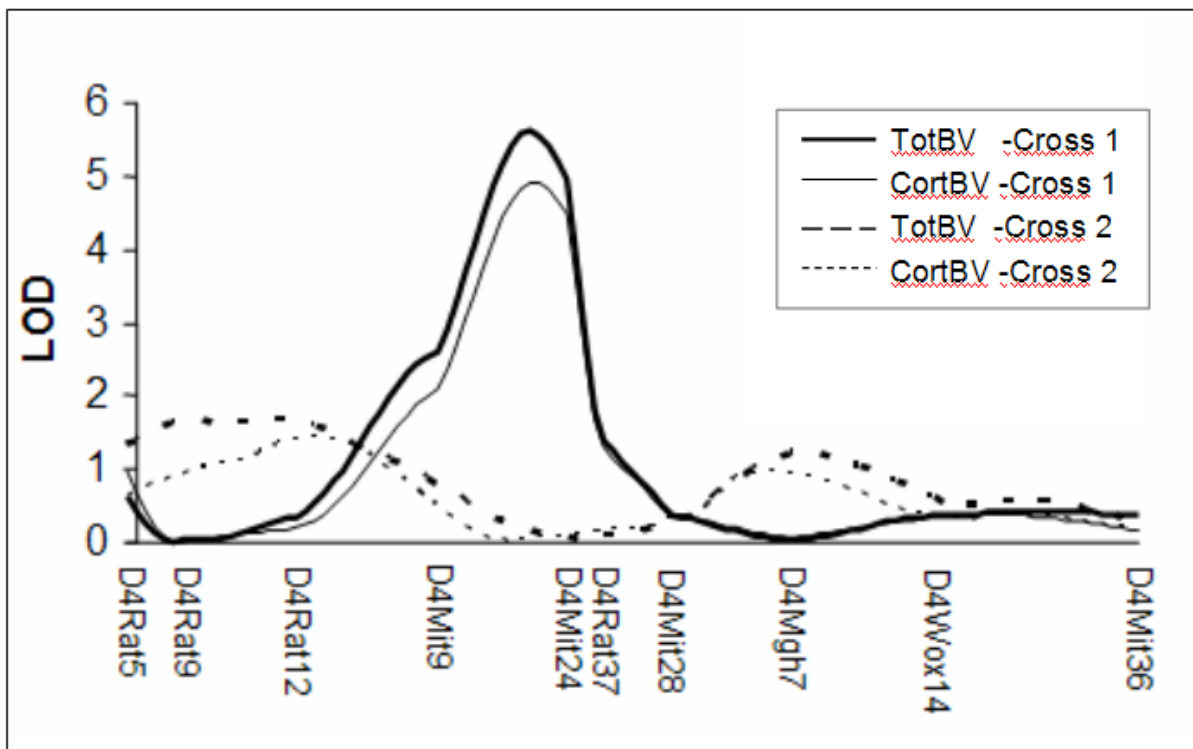


**Fig.3.** Cross-specific QTL on chr 4 in females. The solid lines represent cross 1 carrying the GK mitochondrial DNA, while the broken lines represent cross 2 carrying the F344 mitochondrial DNA.



***Acknowledgement***

This study was supported by grants from the Swedish Research Council (K2006-72X-09109-17-3, 2006-73X-14691-04-3, K2009-53X-14691-07-3), and a Linné grant to Lund University Diabetes Center, Knut och Alice Wallenbergs Stiftelse, Malmö University Hospital Research Foundations, the Medical Faculty of Lund University, Novo Nordisk Foundation, Svenska Diabetesförbundets Forskningsfond, Albert Pålsson Research Foundation, Greta and Johan Kock Foundation and A Osterlund Foundation.

The authors have no conflict of interest to report.

## References

- [1] Peacock M, Turner CH, Econs MJ, Foroud T. Genetics of osteoporosis. *Endocr Rev* 2002;23: 303-26.
- [2] Rivadeneira F, Styrkarsdottir U, Estrada K, Halldorsson BV, Hsu YH, Richards JB, Zillikens MC, Kavvoura FK, Amin N, Aulchenko YS, Cupples LA, Deloukas P, Demissie S, Grundberg E, Hofman A, Kong A, Karasik D, van Meurs JB, Oostra B, Pastinen T, Pols HA, Sigurdsson G, Soranzo N, Thorleifsson G, Thorsteinsdottir U, Williams FM, Wilson SG, Zhou Y, Ralston SH, van Duijn CM, Spector T, Kiel DP, Stefansson K, Ioannidis JP, Uitterlinden AG. Twenty bone-mineral-density loci identified by large-scale meta-analysis of genome-wide association studies. *Nat Genet* 2009;41: 1199-206.
- [3] Bouxsein ML, Uchiyama T, Rosen CJ, Shultz KL, Donahue LR, Turner CH, Sen S, Churchill GA, Muller R, Beamer WG. Mapping quantitative trait loci for vertebral trabecular bone volume fraction and microarchitecture in mice. *J Bone Miner Res* 2004;19: 587-99.
- [4] Eisman JA. Genetics of osteoporosis. *Endocr Rev* 1999;20: 788-804.
- [5] Alam I, Sun Q, Liu L, Koller DL, Carr LG, Econs MJ, Foroud T, Turner CH. Sex-specific genetic loci for femoral neck bone mass and strength identified in inbred COP and DA rats. *J Bone Miner Res* 2008;23: 850-9.
- [6] Koller DL, Alam I, Sun Q, Liu L, Fishburn T, Carr LG, Econs MJ, Foroud T, Turner CH. Genome screen for bone mineral density phenotypes in Fisher 344 and Lewis rat strains. *Mamm Genome* 2005;16: 578-86.
- [7] Lang DH, Sharkey NA, Mack HA, Vogler GP, Vandenberg DJ, Blizard DA, Stout JT, McClearn GE. Quantitative trait loci analysis of structural and material skeletal phenotypes in C57BL/6J and DBA/2 second-generation and recombinant inbred mice. *J Bone Miner Res* 2005;20: 88-99.
- [8] Turner CH, Roeder RK, Wiczorek A, Foroud T, Liu G, Peacock M. Variability in skeletal mass, structure, and biomechanical properties among inbred strains of rats. *J Bone Miner Res* 2001;16: 1532-9.
- [9] Ahmad T, Ohlsson C, Ostenson CG, Kreicbergs A. Peripheral quantitative computed tomography for the detection of diabetic osteopathy: a study in the Goto-Kakizaki rat. *Invest Radiol* 2003;38: 171-6.
- [10] Ahmad T, Ohlsson C, Saaf M, Ostenson CG, Kreicbergs A. Skeletal changes in type-2 diabetic Goto-Kakizaki rats. *J Endocrinol* 2003;178: 111-6.
- [11] Alam I, Sun Q, Liu L, Koller DL, Fishburn T, Carr LG, Econs MJ, Foroud T, Turner CH. Whole-genome scan for linkage to bone strength and structure in inbred Fischer 344 and Lewis rats. *J Bone Miner Res* 2005;20: 1589-96.
- [12] Koller DL, Liu L, Alam I, Sun Q, Econs MJ, Foroud T, Turner CH. Epistatic effects contribute to variation in BMD in Fischer 344 x Lewis F2 rats. *J Bone Miner Res* 2008;23: 41-7.
- [13] Alam I, Sun Q, Liu L, Koller DL, Fishburn T, Carr LG, Econs MJ, Foroud T, Turner CH. Identification of a quantitative trait locus on rat chromosome 4 that is strongly linked to femoral neck structure and strength. *Bone* 2006;39: 93-9.
- [14] Goto Y, Kakizaki M, Masaki N. Production of spontaneous diabetic rats by repetition of selective breeding. *Tohoku J Exp Med* 1976;119: 85-90.
- [15] Galli J, Li LS, Glaser A, Ostenson CG, Jiao H, Fakhrai-Rad H, Jacob HJ, Lander ES, Luthman H. Genetic analysis of non-insulin dependent diabetes mellitus in the GK rat. *Nat Genet* 1996;12: 31-7.

- [16] Ahmad T, Ugarph-Morawski A, Lewitt MS, Li J, Saaf M, Brismar K. Diabetic osteopathy and the IGF system in the Goto-Kakizaki rat. *Growth Horm IGF Res* 2008;18: 404-11.
- [17] Schwartz AV. Diabetes Mellitus: Does it Affect Bone? *Calcif Tissue Int* 2003;73: 515-9.
- [18] Terada M, Inaba M, Yano Y, Hasuma T, Nishizawa Y, Morii H, Otani S. Growth-inhibitory effect of a high glucose concentration on osteoblast-like cells. *Bone* 1998;22: 17-23.
- [19] Zayzafoon M, Stell C, Irwin R, McCabe LR. Extracellular glucose influences osteoblast differentiation and c-Jun expression. *J Cell Biochem* 2000;79: 301-10.
- [20] Gauguier D, Froguel P, Parent V, Bernard C, Bihoreau MT, Portha B, James MR, Penicaud L, Lathrop M, Ktorza A. Chromosomal mapping of genetic loci associated with non-insulin dependent diabetes in the GK rat. *Nat Genet* 1996;12: 38-43.
- [21] Granhall C, Park HB, Fakhrai-Rad H, Luthman H. High-resolution quantitative trait locus analysis reveals multiple diabetes susceptibility loci mapped to intervals <800 kb in the species-conserved Niddm1i of the GK rat. *Genetics* 2006;174: 1565-72.
- [22] Rosengren AH, Jokubka R, Tojjar D, Granhall C, Hansson O, Li DQ, Nagaraj V, Reinbothe TM, Tuncel J, Eliasson L, Groop L, Rorsman P, Salehi A, Lyssenko V, Luthman H, Renstrom E. Overexpression of alpha2A-adrenergic receptors contributes to type 2 diabetes. *Science* 2010;327: 217-20.
- [23] Pravenec M, Hyakukoku M, Houstek J, Zidek V, Landa V, Mlejnek P, Miksik I, Dudova-Mothejzikova K, Pecina P, Vrbacky M, Drahota Z, Vojtiskova A, Mracek T, Kazdova L, Oliyarnyk O, Wang J, Ho C, Qi N, Sugimoto K, Kurtz T. Direct linkage of mitochondrial genome variation to risk factors for type 2 diabetes in conplastic strains. *Genome Res* 2007;17: 1319-26.
- [24] Lagerholm S, Li LS, Jiao H, Park HB, Ohlsson C, Akesson K, Luthman H. Genetic regulation of bone traits is influenced by sex and reciprocal cross in F(2) progeny from GK and F344 rats. *J Bone Miner Res* 2009;24: 1066-74.
- [25] Schlick NE, Jensen-Seaman MI, Orlebeke K, Kwitek AE, Jacob HJ, Lazar J. Sequence analysis of the complete mitochondrial DNA in 10 commonly used inbred rat strains. *Am J Physiol Cell Physiol* 2006;291: C1183-92.
- [26] Seeman E. Pathogenesis of bone fragility in women and men. *Lancet* 2002;359: 1841-50.
- [27] Nilsson M, Johnell O, Jonsson K, Redlund-Johnell I. Quantitative computed tomography in measurement of vertebral trabecular bone mass. A modified method. *Acta Radiol* 1988;29: 719-25.
- [28] Manly KF, Cudmore RH, Jr., Meer JM. Map Manager QTX, cross-platform software for genetic mapping. *Mamm Genome* 2001;12: 930-2.
- [29] Broman KW, Sen S, Owens SE, Manichaikul A, Southard-Smith EM, Churchill GA. The X chromosome in quantitative trait locus mapping. *Genetics* 2006;174: 2151-8.
- [30] Churchill GA, Doerge RW. Empirical threshold values for quantitative trait mapping. *Genetics* 1994;138: 963-71.
- [31] Lander E, Kruglyak L. Genetic dissection of complex traits: guidelines for interpreting and reporting linkage results. *Nat Genet* 1995;11: 241-7.
- [32] Manly KF, Olson JM. Overview of QTL mapping software and introduction to map manager QT. *Mamm Genome* 1999;10: 327-34.
- [33] Weiss LA, Pan L, Abney M, Ober C. The sex-specific genetic architecture of quantitative traits in humans. *Nat Genet* 2006;38: 218-22.
- [34] Lynch M, Walsh B. *Genetics and Analysis of Quantitative Traits*. In. Sunderland, MA, USA: Sinauer Associates, Inc; 1998.

- [35] Holmberg AH, Nilsson PM, Nilsson JA, Akesson K. The association between hyperglycemia and fracture risk in middle age. A prospective, population-based study of 22,444 men and 10,902 women. *J Clin Endocrinol Metab* 2008;93: 815-22.
- [36] Langdahl BL, Uitterlinden AG, Ralston SH, Trikalinos TA, Balcells S, Brandi ML, Scollen S, Lips P, Lorenc R, Obermayer-Pietsch B, Reid DM, Armas JB, Arp PP, Bassiti A, Bustamante M, Husted LB, Carey AH, Perez Cano R, Dobnig H, Dunning AM, Fahrleitner-Pammer A, Falchetti A, Karczmarewicz E, Kruk M, van Leeuwen JP, Masi L, van Meurs JB, Mangion J, McGuigan FE, Mellibovsky L, Mosekilde L, Nogues X, Pols HA, Reeve J, Renner W, Rivadeneira F, van Schoor NM, Ioannidis JP. Large-scale analysis of association between polymorphisms in the transforming growth factor beta 1 gene (TGFB1) and osteoporosis: the GENOMOS study. *Bone* 2008;42: 969-81.
- [37] Ioannidis JP, Ralston SH, Bennett ST, Brandi ML, Grinberg D, Karassa FB, Langdahl B, van Meurs JB, Mosekilde L, Scollen S, Albagha OM, Bustamante M, Carey AH, Dunning AM, Enjuanes A, van Leeuwen JP, Mavilia C, Masi L, McGuigan FE, Nogues X, Pols HA, Reid DM, Schuit SC, Sherlock RE, Uitterlinden AG. Differential genetic effects of ESR1 gene polymorphisms on osteoporosis outcomes. *Jama* 2004;292: 2105-14.
- [38] Alam I, Sun Q, Liu L, Koller DL, Liu Y, Edenberg HJ, Econs MJ, Foroud T, Turner CH. Genomic expression analysis of rat chromosome 4 for skeletal traits at femoral neck. *Physiol Genomics* 2008;35: 191-6.
- [39] Koller DL, White KE, Liu G, Hui SL, Conneally PM, Johnston CC, Econs MJ, Foroud T, Peacock M. Linkage of structure at the proximal femur to chromosomes 3, 7, 8, and 19. *J Bone Miner Res* 2003;18: 1057-65.
- [40] Devoto M, Shimoya K, Caminis J, Ott J, Tenenhouse A, Whyte MP, Sereda L, Hall S, Considine E, Williams CJ, Tromp G, Kuivaniemi H, Ala-Kokko L, Prockop DJ, Spotila LD. First-stage autosomal genome screen in extended pedigrees suggests genes predisposing to low bone mineral density on chromosomes 1p, 2p and 4q. *Eur J Hum Genet* 1998;6: 151-7.
- [41] Duncan EL, Brown MA, Sinsheimer J, Bell J, Carr AJ, Wordsworth BP, Wass JA. Suggestive linkage of the parathyroid receptor type 1 to osteoporosis. *J Bone Miner Res* 1999;14: 1993-9.
- [42] Ralston SH, Galwey N, MacKay I, Albagha OM, Cardon L, Compston JE, Cooper C, Duncan E, Keen R, Langdahl B, McLellan A, O'Riordan J, Pols HA, Reid DM, Uitterlinden AG, Wass J, Bennett ST. Loci for regulation of bone mineral density in men and women identified by genome wide linkage scan: the FAMOS study. *Hum Mol Genet* 2005;14: 943-51.
- [43] Jarvinen TL, Sievanen H, Kannus P, Jarvinen M. Dual-energy X-ray absorptiometry in predicting mechanical characteristics of rat femur. *Bone* 1998;22: 551-8.
- [44] Laib A, Barou O, Vico L, Lafage-Proust MH, Alexandre C, Rugseger P. 3D micro-computed tomography of trabecular and cortical bone architecture with application to a rat model of immobilisation osteoporosis. *Med Biol Eng Comput* 2000;38: 326-32.
- [45] Jamsa T, Jalovaara P, Peng Z, Vaananen HK, Tuukkanen J. Comparison of three-point bending test and peripheral quantitative computed tomography analysis in the evaluation of the strength of mouse femur and tibia. *Bone* 1998;23: 155-61.
- [46] Bower AL, Lang DH, Vogler GP, Vandenbergh DJ, Blizzard DA, Stout JT, McClearn GE, Sharkey NA. QTL analysis of trabecular bone in BXD F2 and RI mice. *J Bone Miner Res* 2006;21: 1267-75.
- [47] Beamer WG, Shultz KL, Ackert-Bicknell CL, Horton LG, Delahunty KM, Coombs HF, 3rd, Donahue LR, Canalis E, Rosen CJ. Genetic dissection of mouse distal chromosome 1 reveals three linked BMD QTLs with sex-dependent regulation of bone phenotypes. *J Bone Miner Res* 2007;22: 1187-96.

[48] Kohler T, Stauber M, Donahue LR, Muller R. Automated compartmental analysis for high-throughput skeletal phenotyping in femora of genetic mouse models. *Bone* 2007;41: 659-67.